ORGANOMETALLICS

Article

pubs.acs.org/Organometallics

Iridium Complexes of N-Heterocyclic Carbene Ligands: Investigation into the Energetic Requirements for Efficient Electrogenerated Chemiluminescence

Bradley D. Stringer,[†] Linh M. Quan,[†] Peter J. Barnard,* David J. D. Wilson, and Conor F. Hogan*

Department of Chemistry, La Trobe Institute for Molecular Science, La Trobe University, Bundoora 3086, Victoria, Australia

Supporting Information

ABSTRACT: A series of five heteroleptic Ir(III) complexes of the general form $Ir(ppy)_2(C^{\wedge}C:)$ have been prepared (C^C represents a bidentate cyclometalated phenyl-substituted imidazolylidene ligand). The five complexes arise from the cyclometalated phenyl ring of the NHC ligand being unsubstituted or having electron-donating (OMe and Me) or electron-withdrawing (Cl and F) groups at the 2- and 4-positions of the ring. The synthesized phenyl-substituted imidazole precursors, imidazolium salts, and Ir(III) complexes have been characterized by elemental analysis, NMR spectroscopy, cyclic voltammetry, and electronic absorption and emission spectroscopy. The molecular structures for two imidazolium salts and two Ir(III) complexes were determined by single-crystal X-ray diffraction. Each of the Ir(III) complexes exhibited intense photoluminescence in acetonitrile solution at room temperature with quantum yields (ϕ_p) ranging from 42% to 68% and excited-state lifetimes on the order of 2 μs. Voltammetric experiments revealed one formal metal-based oxidation process and two ligand-based reductions for each complex. All complexes gave moderate to intense annihilation electrochemiluminescence (ECL); however, only the fluorinated complex produced significant coreactant ECL. The combined electrochemical, spectroscopic, and theoretical investigations offer insights into the reasons for this behavior and suggest useful strategies for the design of ECL emitters. A plot of oxidation potential versus emission color is proposed as a convenient reference guide to aid in the prediction of energy sufficiency in ECL reactions.

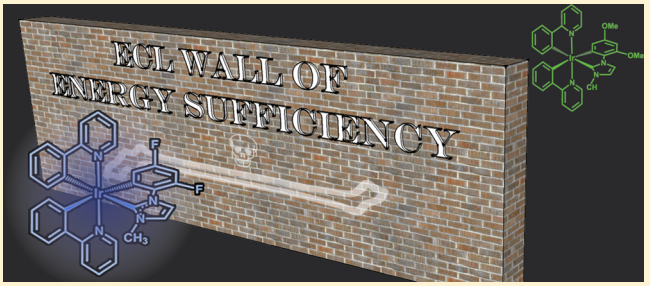

INTRODUCTION

The popularity of N-heterocyclic carbenes (NHCs) has grown rapidly in recent years, such that they have become one of the most widely utilized ligand types in modern organometallic chemistry.[1] NHCs are particularly attractive, as they provide excellent synthetic framework flexibility and NHC-containing complexes often show good stability to air, moisture, and heat.[2] Although NHCs have probably received the most attention for the preparation of homogeneous catalysts,[3] there has been growing interest in the use of these ligands for the development of novel luminescent materials.[4] Luminescent NHC−metal complexes have been prepared for a range of metal ions, including Ru(II),[5] Pt(II),[6] Re(I),[7] and Au(I).[8]

Blue-emitting complexes are sought for applications in light-emitting devices such as organic light-emitting diodes (OLED) and light-emitting electrochemical cells (LECs). In an early study, Forest and co-workers reported the synthesis of homoleptic, tris-cyclometalated Ir(III) complexes of imidazolinylidene- and benzimidazolinylidene-based NHC ligands via a one-pot procedure, which displayed photoluminescence in the near-UV region (~380 nm).[9] These researchers suggested that the use of strong-field ligands, such as carbenes, should result in an increase of the blue phosphorescence efficiency due to a destabilization of thermally accessible nonemissive states. An efficient two-step procedure for the synthesis of homoleptic, tris-cyclometalated Ir(III)−NHC complexes has also been reported.[10] The emission colors of a series of heteroleptic Ir(III) complexes with either cyclometalated benzimidazolinylidene-[11] or imidazolinylidene-based[12] NHC ligands were tuned through modification of the chelating NN: ancillary ligand. Cationic Ir(III) complexes with two cyclometalated 2-(phenyl)-pyridine ligands and one chelating NHC−pyridine ancillary ligand, which have a range of emission wavelengths, have been reported.[13]

Electrochemiluminescence or electrogenerated chemiluminescence (ECL), where luminescent emission is initiated electrochemically, is an area of growing importance in analytical science.[14] In ECL reactions the excited state of the luminophore is populated when an electron is transferred from a powerful reductant to the lowest unoccupied molecular orbital (LUMO; usually a ligand-based π^* orbital) of the oxidized complex. The reductant may be derived from either the reduction of the metal complex itself, referred to as annihilation ECL, or from a sacrificial reagent, in which case it is called coreactant ECL. The application of coreactant ECL as

Special Issue: Organometallic Electrochemistry

Received: January 24, 2014
Published: May 27, 2014

   dx.doi.org/10.1021/om500076w | Organometallics 2014, 33, 4860−4872

the basis for highly sensitive immunoassays has been predominantly based on the use of tris(2,2′-bipyridine)-ruthenium(II) ($[Ru(bpy)_3]^{2+}$) and its derivatives, the vast majority of which emit in a narrow wavelength range around 600 nm.[14c,15] In contrast, relatively few green and blue ECL emitters are available, and the most effective design of blue-emitting complexes for ECL detection is an important area of current research. Since the early work of Wightman,[16] Richter,[17] and Kapturkiewicz,[18] interest in the ECL of cyclometalated iridium complexes has grown steadily due to their efficient luminescence and tunable emission properties. We are interested in the development of new ECL-based sensing materials with varying emission and redox characteristics for their potential application in multiplexed sensing. N-heterocyclic carbene based complexes are potentially useful in this regard: a wide variety of ligands can be readily prepared due to the framework flexibility of the NHC moiety. Moreover, the electronic properties of NHC ligands can be easily tuned through the choice of the azole precursor as well as the wing-tip substituents.

In the search for new luminescent and ECL active materials we have undertaken a combined electrochemical, spectroscopic, and theoretical investigation of a series of green-/blue-emitting Ir(III) complexes. The synthesized Ir(III) complexes were of the general form $Ir(ppy)_2(C^\wedge C:)$ (where ppy represents cyclometalated 2-(phenyl)pyridine and C^C: represents a cyclometalated phenyl-substituted imidazolylidene ligand). The NHC ligands were derived from a series of 2,4-disubsituted phenylimidazolium salts, where the substituents on the phenyl ring were modified to provide both electron-donating and electron-withdrawing character. Electrochemical and spectroscopic studies show how the electron density at the metal center was modulated by these structural modifications to the cyclometalated phenyl group of the NHC ligand. We report for the first time a description of the ECL properties of NHC-based iridium complexes. The results of these studies, combined with theoretical studies, provide insight not only into the electronic structure of these new complexes but also into the electronic structure of these new complexes but also into the energetic requirements for efficient ECL in general.

RESULTS AND DISCUSSION

Synthesis. The 2,4-disubsituted phenylimidazoles **1**−**5** were obtained in moderate to good yield via a two-step procedure involving initial reaction of an equimolar mixture of glyoxal with the chosen disubstituted aniline, followed by the addition of NH_4Cl and ring closure with formaldehyde (Scheme 1).[14d] Formation of the desired imidazolium salts **6**−**10** (Scheme 2) was achieved via alkylation of the 2,4-disubsituted phenyl-

Scheme 1. Synthesis of 2,4-Substituted Phenylimidazoles 1−5

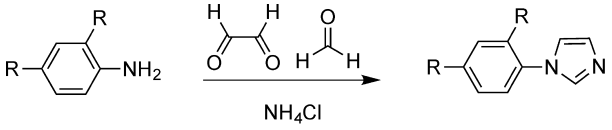

Compound	R	Yield
1	H	64%
2	Me	48%
3	OMe	53%
4	Cl	85%
5	F	49%

Scheme 2. Synthesis of 2,4-Substituted Azolium Salts 6−10

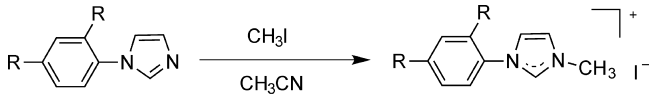

Compound	R	Yield
6	H	80%
7	Me	86%
8	OMe	77%
9	Cl	79%
10	F	82%

imidazoles **1**−**5** with iodomethane in acetonitrile. The unsubstituted imidazolium salt precursor **1** has been described previously.[14d]

The $Ir(ppy)_2(C^\wedge C:)$ complexes **11**−**15** (the bidentate imidazolylidene ligands are derived from the imidazolium salts **6**−**10**, respectively) were prepared by heating the chosen imidazolium salt with the chloro-bridged Ir(III) dimeric precursor compound $[Ir(ppy)Cl]_2$ and Ag_2O in 1,2-dichloroethane (Scheme 3). Early attempts to carry out this reaction at

Scheme 3. Synthesis of Iridium(III) Complexes 11−15

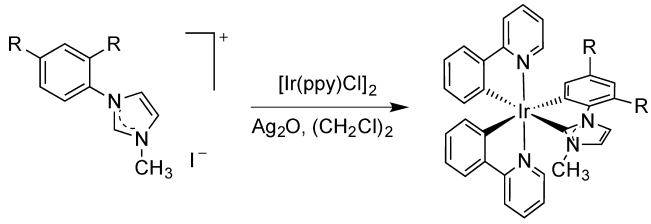

Complex	Azolium salt	R	Yield
11	**6**	H	87%
12	**7**	Me	73 %
13	**8**	OMe	42%
14	**9**	Cl	86%
15	**10**	F	38 %

~60 °C in solvents commonly used for NHC/Ag(I) transmetalation reactions (e.g., CH_2Cl_2 and CH_3OH) produced very low yields (<2%) of the desired complexes, with the starting materials being isolated. Employing the higher boiling solvent 1,2-dichloroethane in combination with an increased reaction temperature (95 °C) produced complexes **11**−**15** in good yields.

Characterization. The structures of the 2,4-disubstituted phenylimidazoles, the imidazolium salts and the $Ir(ppy)_2(C^\wedge C:)$ complexes were confirmed by ^1H and ^{13}C NMR spectroscopy and, in the case of the **9**, **10**, **12**, and **15**, by X-ray crystallography. The imidazolium salts gave relatively simple ^1H NMR spectra, all with a characteristic downfield resonance for the strongly deshielded pro-carbenic proton, which occurred at 9.75, 10.09, 9.97, 10.19, and 10.36 ppm for **6**−**10**, respectively.

The synthesized $Ir(ppy)_2(C^\wedge C:)$ complexes **11**−**15** were uncharged, with two cyclometalated 2-(phenyl)pyridine ligands in addition to the 2,4-disubstituted phenyl imidazolylidene ancillary ligand coordinated to the Ir(III) center. The predicted number of signals were obtained in the ^1H and ^{13}C NMR spectra for the $Ir(ppy)_2(C^\wedge C:)$ complexes, consistent with the low-symmetry structures. As is generally observed for systems of this type,[19] the mutually trans disposition of the pyridyl groups of the ppy ligands found in the precursor compound

dx.doi.org/10.1021/om500076w | Organometallics 2014, 33, 4860−4872

$[Ir(ppy)Cl]_2$ was retained in the $Ir(ppy)_2(C^{\wedge}C:)$ complexes that formed. As expected, upon deprotonation and coordination of the NHC group the signal for the imidazolium salt pro-carbenic proton was absent from the ^1H NMR spectra of the complexes. In addition a characteristic downfield chemical shift was observed for the carbenic carbon atom, occurring at 176.21, 178.36, 174.82, 178.47, and 176.32 ppm for complexes **11**–**15**, respectively.

Structural Studies. Crystallographic data for the imidazolium salts **9** and **10** and the Ir(III) complexes **12** and **15**, are given in Table S1 (Supporting Information) with selected bond distances collated in Table 1. The X-ray crystal structures for **9** and **10** are illustrated in Figure 1. For compound **9**, a short hydrogen-bonding interaction of 2.7572(2) Å is observed between the weakly acidic pro-carbenic proton (C11) and the iodide counterion (I2).

Table 1. Selected Bond Distances (Å) from the X-ray Structures of Imidazolium Salts 9 and 10 and Iridium(III) Complexes 12 and 15

	9	10	12	15
C1–N1	1.334(3)	1.331(3)	1.377(5)	1.367(4)
C1–N2	1.327(3)	1.320(3)	1.355(5)	1.356(4)
Ir1–C1			2.053(4)	2.063(3)
Ir1–C4			2.106(4)	2.091(3)
Ir1–C11			2.038(4)	2.036(3)
Ir1–C22			2.065(4)	2.059(3)
Ir1–N3			2.039(3)	2.040(2)
Ir1–N4			2.045(3)	2.050(2)

The X-ray crystal structures of the Ir(III) complexes **12** and **15** are illustrated in Figure 2. Both complexes display a slightly distorted octahedral coordination geometry about the Ir(III) centers with two cyclometalated 2-(phenyl)pyridine ligands in combination with the cyclometalated phenyl-substituted imidazolylidene unit. As expected for the ppy ligands, the pyridyl groups and phenyl groups adopt mutually trans and cis dispositions, respectively. The $Ir-C_{carbene}$ (Ir1–C1) bond distances are similar for each complex, being 2.053(4) and 2.063(4) Å for **12** and **15**, respectively. Comparable $Ir-C_{carbene}$ bond distances have been reported previously for imidazolylidene-containing complexes. For example, the $Ir-C_{carbene}$ bond distance for the Ir(III) complex of a pyridyl-substituted NHC ligand in combination with two cyclometalating 2-(2,4-difluorophenyl)pyridine ligands is 2.060(5) Å.[13c] Shorter $Ir(III)-C_{carbene}$ bond distances of 1.91 and 1.97 Å were reported for a homoleptic Ir(III) complex of a cyclometalated imidazolylidene-based NHC ligand.[10]

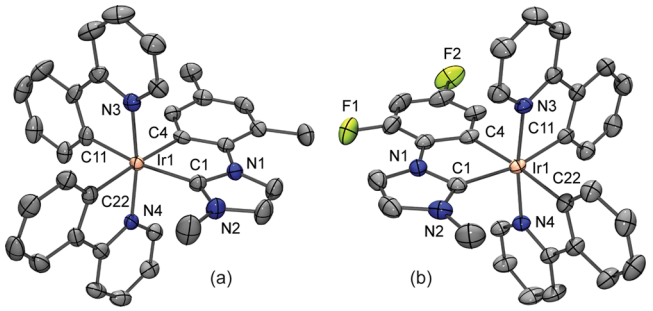

Figure 2. ORTEP[20] representations of the X-ray crystal structures of the Ir(III) complexes (a) **12** and (b) **15**. The hydrogen atoms and solvents of crystallization have been omitted for clarity. Thermal ellipsoids are shown at 50% probability.

Absorption Spectroscopy. The UV–visible absorbance spectra for compounds **11**–**15** (Figure 3 and Table 2) show intense absorption bands below 300 nm due to spin-allowed $\pi \rightarrow \pi^*$ ligand-centered (LC) transitions originating on the NHC and phenylpyridine ligands. The low-intensity bands between 500 and 300 nm can be assigned to both allowed and spin-forbidden metal-to-ligand charge transfer (MLCT) transitions. Strong spin–orbit coupling of the metal center promotes mixing of these charge-transfer transitions with the higher energy spin-allowed ligand-centered transitions.[21] For complexes **14** and **15** the strongly electron withdrawing groups on

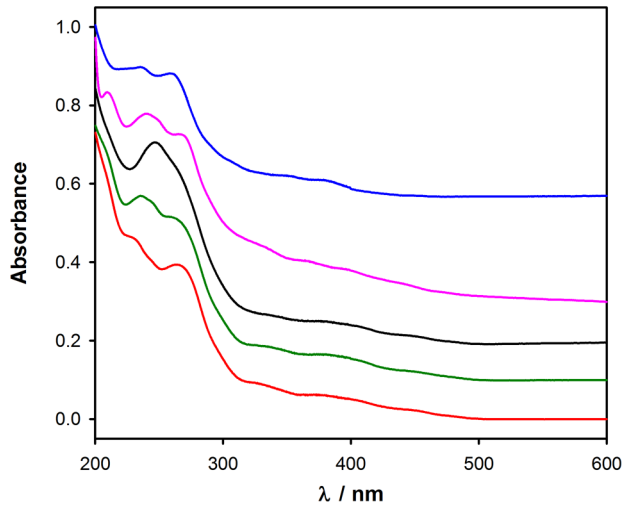

Figure 3. Absorbance spectra of 10^{-5} M solutions of complexes **11**–**15** (bottom to top) dissolved in acetonitrile. Spectra are offset for clarity.

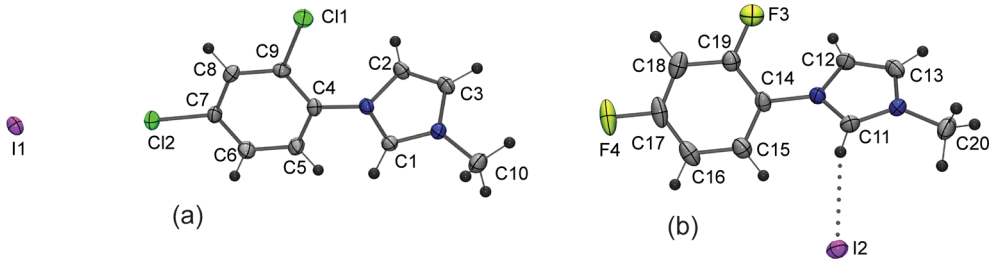

Figure 1. ORTEP[20] representations of the X-ray crystal structures of the imidazolium salts (a) **9** and (b) **10**. Thermal ellipsoids are shown at 50% probability.

dx.doi.org/10.1021/om500076w | *Organometallics* 2014, 33, 4860–4872

Table 2. Spectroscopic Properties of Ir(III) Complexes 11−15 in Comparison with Those of $[Ru(bpy)_3]^{2+}$ [a]

	λ_{max}/nm (ε/M^{-1} cm^{-1})[b]	photoluminescence λ_{max}/nm[c]	quantum yield ϕ_p[d]	lifetime τ_p/μs	radiative rate const $k_r/10^5$ s^{-1}[e]	nonradiative rate const $k_{nr}/10^5$ s^{-1}
11	237 (43100), 271 (37900), 334 (8500), 379 (6100), 408 (4500 sh), 450 (2200 sh)	529	0.498	1.98	2.5	2.5
12	240 (45700), 270 (38500), 337 (8200), 382 (6300), 408 (4700 sh), 450 (2100 sh)	533	0.420	1.59	2.6	3.6
13	255 (48000), 271 (39000 sh), 380 (4900), 409 (3400 sh), 450 (1100 sh)	525	0.621	1.97	3.2	1.9
14	215 (51500), 244 (48400), 273 (41600), 368 (11100 sh), 401 (8800), 445 (5200 sh)	507	0.683	2.03	3.4	1.6
15	243 (31100), 267 (28300), 353 (4900 sh), 384 (3600)	487	0.531	2.06 (0.64)[f]	2.6 (8.3)	2.3 (7.4)
$[Ru(bpy)_3][PF_6]_2$	208 (46300 sh), 244 (27000), 253 (23300), 286 (82400), 324 (9300), 353 (5400), 424 (11000 sh), 450 (13600)	620	0.087	0.85	1.0	10.7

[a]All complexes 1×10^{-5} M in acetonitrile. [b]λ_{max} is the position of the peak or shoulder in the absorbance or emission profile, and $\boldsymbol{\varepsilon}$ is the molar absorptivity. [c]Emission corrected for variation in detector sensitivity with wavelength. [d]Absolute quantum yields. The 95% confidence intervals (n = 6) were no larger than ±0.0035. [e]Radiative rate constant $k_r = \phi_p/\tau_p = 1/\tau^0$ and nonradiative rate constant $k_{nr} = (1 - \phi_p)/\tau_p$, where the intrinsic lifetime $\tau^0 = \tau_p/\phi_p$. [f]Double-exponential decay (longer lifetime component 60%).

the auxiliary NHC ligand result in the onset of these MLCT bands being blue-shifted (10−50 nm) relative to the other complexes.

Photoluminescence. The photoluminescence from the Ir(III) complexes arises from the excitation of an electron from the HOMO, which is partially metal based and partially located on the phenyl moieties of the two phenylpyridine ligands, to a ligand-based π^* antibonding orbital. The excited state is therefore best described as an admixed metal−ligand/intra-ligand charge transfer (MLCT/LLCT). Initial excitation is followed by intersystem crossing to the lowest triplet state, from which emission occurs.

Each of the iridium(III) complexes exhibited intense photoluminescence in dilute acetonitrile solution at room temperature, with quantum yields (ϕ_p) ranging from 42% to 68%, increasing in the order **14** > **13** > **15** > **11** > **12** (Table 2 and Figure 4a). The kinetic parameters for luminescence decay (Table 2) suggest that the differences in quantum yield between the complexes may be due to differences in the rate of a nonradiative reaction, as k_{nr} follows the opposite trend to ϕ_p and, with the exception of **15**, obeys the energy gap law (Figure S2, Supporting Information). The deactivation route process may also comprise thermal deactivation to a dissociative ^{3}MC state, as suggested by Thompson et al. for other tris-cyclometalated iridium complexes.[22]

As is often observed for other cyclometalated iridium complexes,[22] the photoluminescence intensities were found to be extremely sensitive to the presence of oxygen even in minute amounts. This necessitated a very high level of care to maintain anaerobic conditions during quantum yield and lifetime determinations. Photoluminescence decay profiles are shown in Figure S1 (Supporting Information). The excited-state lifetimes for the iridium complexes, calculated from these transients, were all between 1.6 and 2.1 μs, which is approximately twice as long as that measured for $[Ru(bpy)_3]^{2+}$. This is one factor which undoubtedly contributes to the high sensitivity to oxygen quenching, in comparison with the ruthenium complex.

The corrected photoluminescence spectra for the iridium complexes in deaerated CH_3CN at room temperature are shown in Figure 4. For complexes **11**−**13** the emission color shows little variation. However, as shown by the data presented in Table 2, the two halogenated complexes, **14** and **15**, are blue-shifted significantly (by about 25 and 50 nm, respectively).

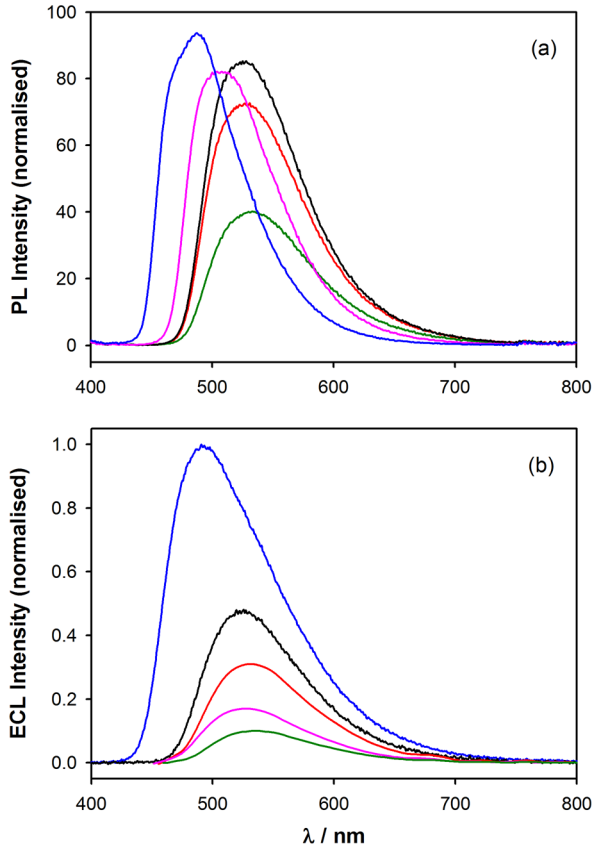

Figure 4. (a) Photoluminescence spectra for 10^{-6} M solutions of the iridium complexes in acetonitrile: (red) **11**; (green) **12**; (black) **13**; (pink) **14**; (blue) **15**. The integrated emission intensity in each case has been normalized for the absorbance of the solution at the wavelength of excitation (345 nm) reflecting relative photoluminescence quantum efficiencies. (b) ECL spectra produced via annihilation between the oxidized and reduced forms of the complexes. All iridium complexes are 10^{-4} M solutions in acetonitrile containing 0.1 M $[Bu_4N][PF_6]$. Intensities have been normalized to reflect relative ECL quantum efficiencies.

These observations may be accounted for by considering electron resonance and inductive effects. The electron-withdrawing halogen groups are positioned meta to the metal coordination site and therefore inductively stabilize the

dx.doi.org/10.1021/om500076w | Organometallics 2014, 33, 4860−4872

Table 3. Electrochemical and Electrochemiluminescence Properties of Iridium Complexes 11−15 in Comparison with Those of $[Ru(bpy)_3]^{2+}$ [a]

	anodic process E°_{ox}/V	cathodic process E°_{red}/V	$E^\circ_{ox} - E^\circ_{red}$/V	$10^6 D$ [b]/cm^2 s^{-1}	λ_{max} ECL [c]/nm	rel annihilation ECL intensity ϕ_{ECL} [d]	rel coreactant ECL intensity ϕ_{ECL} [e]
11	0.24	−2.72, −2.98	2.96	8.43	532	31	0
12	0.21	−2.73, −3.00	2.95	7.79	537	10	0
13	0.25	−2.72, −2.98	2.98	7.44	531	48	0
14	0.36	(−2.61), −2.70, −2.97	2.97	10.4	524	17	0.1
15	0.66	−2.57, −2.82	3.23	5.54	490	103	20
$[Ru(bpy)_3]^{2+}$	0.89	−1.73, −1.92, −2.16	2.62	7.90	618	100	100

[a] 0.2 mM/0.1 M $(Bu_4N)PF_6$ in acetonitrile. Potentials referenced to Fc/Fc^+. [b] Diffusion coefficients calculated from plots of peak current vs square root of scan rate. A representative Randles−Sevçik plot is shown in the Supporting Information (Figure S3). [c] Spectra from annihilation ECL experiments. [d] Relative ECL efficiency via annihilation. [e] Relative coreactant ECL efficiency.

HOMO, which is substantially based on the iridium center (see Figure 6). The effect is to increase the HOMO−LUMO gap and thus the emission energy. Therefore, a blue shift in **14** and **15** is observed when chlorine or fluorine groups are substituted at the 2- and 4-positions of the phenyl group on the auxiliary ligand. On the other hand, no shift is observed in the case of the methoxy-substituted complex **13** because this group exerts a resonance effect and would therefore need to be situated ortho/para to the coordination site to exert an influence on the HOMO.

Electrochemistry. The electrochemical properties of **11**−**15** were studied using cyclic voltammetry, and the results are summarized in Table 3. Figure 5 shows the cyclic voltammograms (CVs) of **11**−**15** and $[Ru(bpy)_3]^{2+}$ in oxygen-free acetonitrile. When scanned anodically, each complex exhibited a one-electron-oxidation process, which can be formally assigned to the Ir^{III}/Ir^{IV} redox couple, though it should be noted that the HOMO is also delocalized over the phenyl moieties of the phenylpyridine ligands (see Figure 6). In the case of **15** this oxidation couple was fully chemically reversible, with forward and reverse peaks the same magnitude ($i_{p,ox} = i_{p,red}$) at all scan rates tested (0.1−5.0 V s^{-1}), whereas the responses for **11** and **13** were reversible only at higher scan rates (≥1.0 V s^{-1}) and the responses for **12** and **14** exhibited only semireversible behavior regardless of scan rate.

Scanning in the cathodic region typically resulted in two reversible, one-electron waves which are assigned to the stepwise reduction of the two ppy ligands on the basis of previous results for similar compounds such as $Ir(ppy)_3$ (which has a reduction potential of −2.67 V vs Fc).[23] This conclusion is also supported by the theoretical data presented later (see Figure 6). Complex **14** also displayed a third irreversible peak at −2.61 V, the shape of which suggests that it is related to adsorption of the complex on the electrode.

The CVs in Figure 4 indicate that the oxidation and reduction potentials of the Ir(III) complexes are all considerably more negative than those of $[Ru(bpy)_3]^{2+}$. While the oxidation potential (E°_{ox}) and reduction potential (E°_{red}) for **11**−**13** are all quite similar, substitution of electronwithdrawing groups on the ancillary ligand caused a positive shift in E°_{ox}: by 120 mV in the case of the dichloro-substituted **14** and by 420 mV in the case of the difluoro-substituted **15**. With halogen substitution at the NHC ligand the effect on reduction potentials was comparatively modest, resulting in a positive shift in E°_{red} by 20 mV for **14** and 150 mV for **15**.

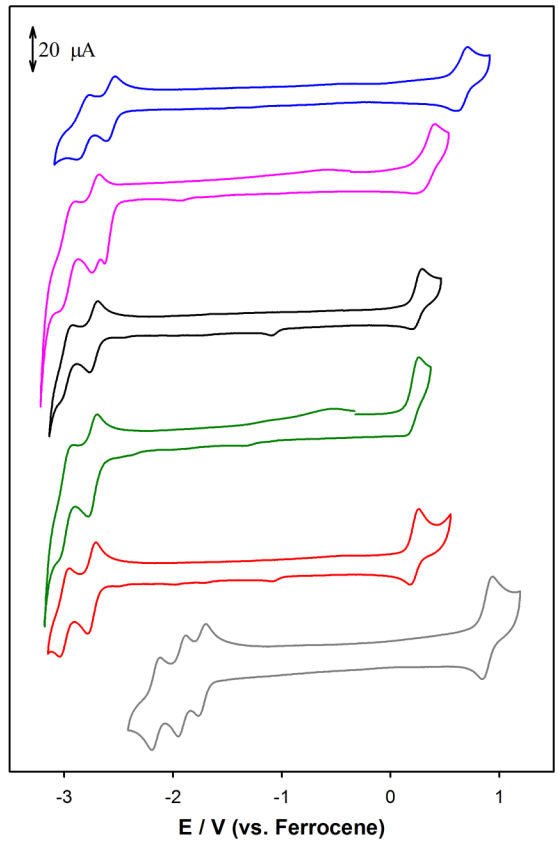

Figure 5. Cyclic voltammetric responses for (top to bottom) **15**, **14**, **13**, **12**, **11**, and $[Ru(bpy)_3]^{2+}$ using a glassy-carbon-disk working electrode (3 mm diameter) at a scan rate of 1.0 V s^{-1}. The concentration was 0.2 mM in each case for the samples dissolved in acetonitrile containing 0.1 M $[Bu_4N][PF_6]$ as supporting electrolyte.

It is notable that the electrochemical HOMO−LUMO gap ($E^\circ_{ox} - E^\circ_{red}$) (see Table 3) correlates very well with the emission energies of the complexes. The electrochemical results therefore provide a basis for understanding the luminescence data presented in Table 2. For example, in light of the oxidation potential data, the blue shifts observed for the luminescence maxima of **14** and **15** can be understood as resulting from a widening of the HOMO−LUMO gap caused by stabilization of the HOMO energy levels of these complexes. In both complexes, the HOMO stabilization effect dominates the relatively small LUMO stabilizations evident in the reduction potentials.

dx.doi.org/10.1021/om500076w | Organometallics 2014, 33, 4860−4872

Theoretical Calculations. The optimized geometries of complexes **11**−**15** maintain a common framework with little variation due to the R substituent. For R = OMe, a conformational search was carried out in order to identify the lowest energy structure. Both M06-2X and mPW1PW91 DFT methods yielded equivalent geometries. Geometrical parameters are consistent with the X-ray structures (Table 1): mPW1PW91/def2-SVP calculated bond distances for **15** are Ir1−C1 = 2.102 Å, C1−N1 = 1.367 Å, and C1−N2 = 1.355 Å, in comparison to 2.063, 1.367, and 1.356 Å, respectively, from the X-ray structure. Similarly, for **12** the calculated and X-ray derived structures are in excellent agreement. The mPW1PW91/def2-SVP geometries are provided in the Supporting Information as a text file of all computed molecule Cartesian coordinates in .xyz format for convenient visualization.

Molecular orbitals (MOs) were calculated with the inclusion of solvent effects and with the def2-TZVP basis set, which yielded much better agreement with experimental trends than gas-phase results. Only solvent-corrected results are presented. There is significant DFT functional dependence for the MO energies and HOMO−LUMO gaps, although the relative trends always remain consistent. The mPW1PW91 and PBE functionals yielded MO energies within 0.01 eV of each other. In comparison, the B3LYP and BP86 functionals consistently predicted smaller HOMO−LUMO gaps than did mPW1PW91: 0.4 eV lower with B3LYP and 1.7−1.8 eV with BP86. M06-2X and ωB97XD functionals yielded larger HOMO−LUMO gaps than mPW1PW91: 1.8−1.9 eV larger with M06-2X and 3.2 eV with ωB97XD. The Hartree−Fock calculated HOMO−LUMO gaps were 5.6−5.7 eV higher in energy, resulting from much lower HOMO energies and much higher LUMO energies. These trends are consistent with those we recently reported for a series of blue-emitting Ir(III) complexes.[24]

Basis set effects were further investigated with the addition of diffuse functions to def2-TZVP. Augmenting with diffuse functions altered mPW1PW91 frontier MO energies by only 0.03 eV and the HOMO−LUMO gap by 0.01 eV, which is not significant. For comparison with experiment and subsequent analysis of MO energies only mPW1PW91/def2-TZVP solvent-corrected results are considered.

Contour plots of the MOs indicate very similar properties for the Ir(III) complexes (see Figure 6 and Figure S4 in the Supporting Information). For all iridium complexes the LUMO (and LUMO+1 to LUMO+3) is located on the phenylpyridine ligand. The HOMO is predominantly centered on the metal d orbital and the phenylpyridine ligand, while with R = OMe (**15**) there is additional contribution from the auxiliary NHC ligand. The HOMO-1 has contributions from the metal d orbital and the auxiliary ligand. The nature of the frontier MOs was further characterized from a Mulliken population analysis as a function of molecular fragments (metal, phenylpyridine, and auxiliary NHC ligand). As with the MO energies, the nature of the frontier MOs also exhibited a functional dependence, although it was limited to differences in the nature of the HOMO. Both BP86 and mPW1PW91 functionals produced similar trends; however, it is notable that the BP86 functional consistently predicts a 10% larger metal contribution to the HOMOs for the iridium complexes. All methods predict that the LUMO for all of the iridium complexes is entirely ppy based (>95%). Plots of the fragment contribution (metal, ppy, or NHC-based ligand) to the LUMO and HOMO are included in Figures S5 and S6 (Supporting Information).

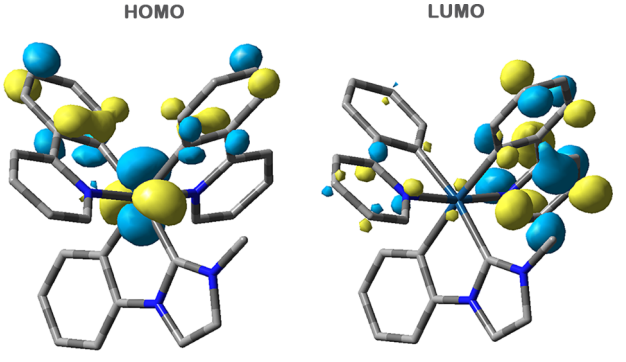

Figure 6. HOMO and LUMO for **11**. Hydrogen atoms are omitted for clarity. The complete set of orbitals for each complex can be seen in the Supporting Information (Figure S4).

TDDFT calculations confirm the assignment of UV−visible bands; the most intense bands below 300 nm are principally transitions from low-lying ligand-based π orbitals (typically HOMO-6) to the LUMO (π^*) centered on the ppy ligand.

Electrochemiluminescence. All five complexes exhibited intense to moderately intense ECL via the annihilation mechanism.[14b] As illustrated in Figure 4b, the ECL emission profiles are essentially identical with the photoluminescence spectra, indicating that the same excited state for each complex is populated regardless of whether an optical or electrochemical excitation method is employed. To accurately quantify the ability of these complexes to produce ECL, their relative annihilation ECL efficiencies were measured from potential step experiments where the reduced and oxidized forms were generated sequentially at the working electrode according to

$$[\mathrm{Ir(ppy)_2(L)}] \rightarrow [\mathrm{Ir(ppy)_2(L)}]^+ + \mathrm{e}^- \quad (1)$$

$$[\mathrm{Ir(ppy)_2(L)}] + \mathrm{e}^- \rightarrow [\mathrm{Ir(ppy)_2(L)}]^- \quad (2)$$

$$[\mathrm{Ir(ppy)_2(L)}]^- + [\mathrm{Ir(ppy)_2(L)}]^+ \rightarrow [\mathrm{Ir(ppy)_2(L)}]^* + [\mathrm{Ir(ppy)_2(L)}] \quad (3)$$

$$[\mathrm{Ir(ppy)_2(L)}]^* \rightarrow [\mathrm{Ir(ppy)_2(L)}] + h\nu \quad (4)$$

where L is the bidentate C^C: imidazolylidene-based NHC ligand. As indicated in Table 3, **15** produced the highest annihilation ECL intensity, slightly exceeding that of $[\mathrm{Ru(bpy)^3}]^{2+}$. The annihilation ECL efficiencies of the other compounds varied from 10 to 48% relative to the standard.

In the case of coreactant ECL using tripropylamine (TPA), the excited state is generated via the following mechanism, after generation of $[\mathrm{Ir(ppy)_2(L)}]^+$ via reaction 1:

$$\mathrm{TPA} \rightarrow \mathrm{TPA}^{\bullet+} + \mathrm{e}^- \quad (5)$$

$$\mathrm{TPA}^{\bullet+} \rightarrow \mathrm{TPA}^{\bullet} + \mathrm{H}^+ \quad (6)$$

$$[\mathrm{Ir(ppy)_2(L)}]^+ + \mathrm{TPA}^{\bullet} \rightarrow [\mathrm{Ir(ppy)_2(L)}]^* + \mathrm{P} \quad (7)$$

followed by de-excitation via reaction 4

Interestingly, despite the strong annihilation ECL observed for the complexes, only **15** produced significant emission via the coreactant pathway; the ECL emission efficiency was 20% for this complex with respect to the ruthenium-based standard

These observations provide an interesting insight into the importance of energetic considerations in the design of novel electrochemiluminophores, and in particular the interplay of

dx.doi.org/10.1021/om500076w | Organometallics 2014, 33, 4860−4872

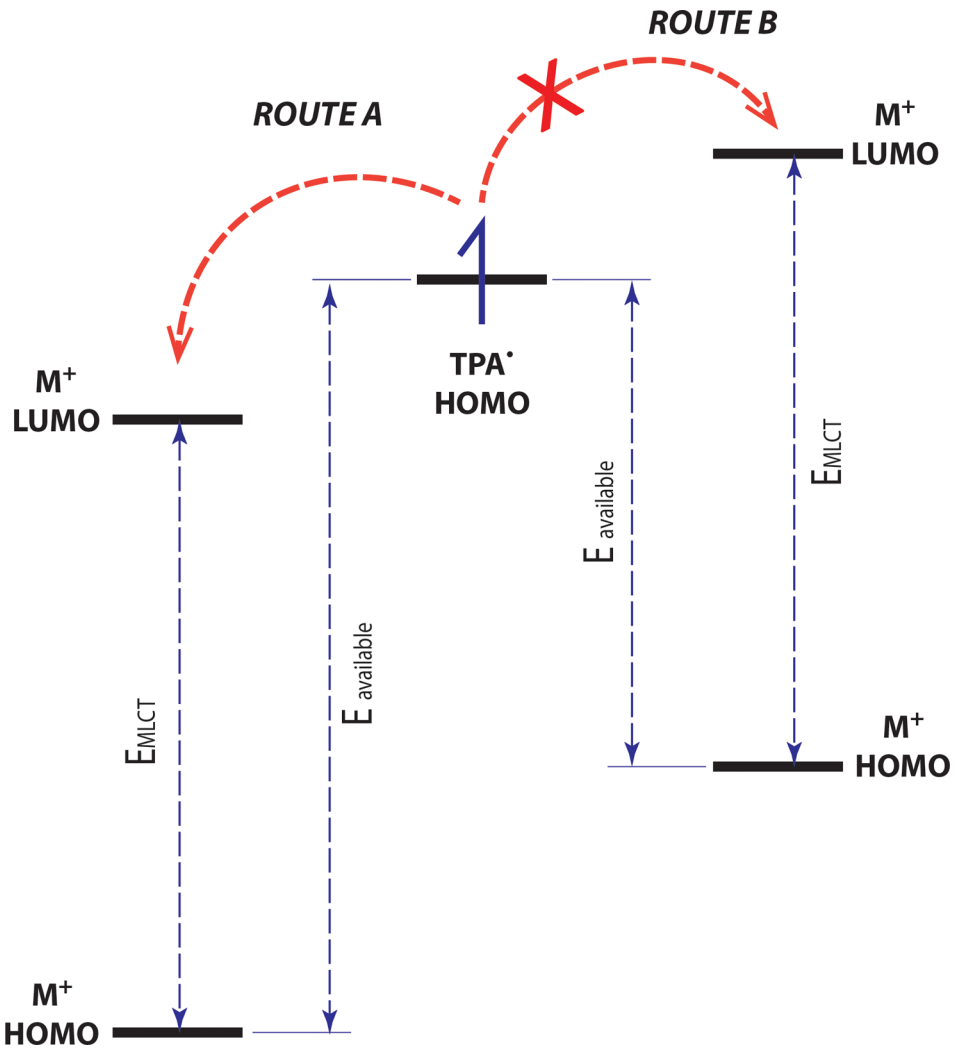

Figure 7. Energy diagram for coreactant ECL (reaction 7 in the text): (route A) energy-sufficient coreactant ECL system where $E^{\circ}_{ox} > E_{critical}$; (route B) energy-insufficient coreactant ECL system where $E^{\circ}_{ox} < E_{critical}$.

spectroscopic and electrochemical properties in such systems. For example, the free energy (ΔG) associated with annihilation reaction (3) above may be estimated using the relationship

$$\Delta G = E^{\circ}_{red} - E^{\circ}_{ox} + E_{MLCT} \quad (8)$$

where E_{MLCT} is the spectroscopic energy of the excited state in eV, which is best taken from the λ_{max} value of the low-temperature emission spectrum (but may be derived from room-temperature data to a first approximation). As the values for E_{MLCT} for complexes **11**−**15** vary in the range 2.35−2.55 eV, it is clear that the annihilation reaction (3) between the reduced and oxidized species leading to the excited state is energy sufficient in each case, with **15** having the most negative value of ΔG and exhibiting the greatest ECL efficiency.

In the case of the coreactant ECL pathway the electro-reduced complex is replaced by a reducing radical species derived from the coreactant (TPA$^{\bullet}$), and the ΔG value of the reaction may be estimated from

$$\Delta G = E^{\circ}(TPA^{\bullet}) - E^{\circ}_{ox} + E_{MLCT} \quad (9)$$

where E°(TPA$^{\bullet}$), the reduction potential of the radical, has previously been found to have a value of −2.1 V vs Fc.[23,25] Substituting the values of E°_{ox} from Table 3 and the values of E_{MLCT} derived from the emission peak maxima in Table 2 into eq 9 shows that the ECL reaction (eq 7) for the cases of **11**−**13** does not have sufficient energy to populate the excited state while that for **14** is only marginally energy sufficient. This explains why the last four complexes (**11**−**14**) give little or no coreactant ECL emission, whereas **15**, for which the reaction is energy sufficient by about 0.2 eV according to eq 9, gives relatively intense emission.

These observations are in accord with those of Kapturkiewicz et al., who gave a detailed account of how the efficiency of Ir(ppy)$_3$ ECL depended on the available energy supplied by reaction with various electroreduced aromatic nitriles and ketones.[18a] On the basis of eq 9 it is clear that, when seeking to design new electrochemiluminophores for applications such as ECL-based assays, it is necessary to optimize the energetics of the ECL reaction (7) so as to achieve maximum ECL efficiency and therefore enhance sensitivity. However, unlike the case with the model systems investigated by Kapturkiewicz et al.,[18a] there is little scope to vary the reducing power of the coreactant radical. This is because, in order to function in aqueous-based assays, the reductant must be capable of being produced oxidatively as in eqs 5 and 6. Therefore, the best strategy is to focus on increasing the oxidizing ability of the luminophore.

Apart from optimizing sensitivity, an increasingly important goal in the field of ECL detection is the development of

dx.doi.org/10.1021/om500076w | *Organometallics* 2014, 33, 4860−4872

electrochemiluminophores with varying emission wavelengths for applications such as multiplex analysis.[26] An important consideration here is that higher energy emitters place greater demands on the energy requirements of the ECL reaction. In other words, the bluer the emission, the greater the amount of energy that must be available from reaction 7 in order to populate the excited state. Figure 7 illustrates this point clearly: for a given emission color (and E_{MLCT} value), the oxidation potential must be sufficiently positive (*and* the reduction potential sufficiently positive) such that the electron transfer from the HOMO of TPA$^{\bullet}$ to the LUMO of the complex is energetically favorable. Note that, according to Marcus−Hush theory, the more positive the value of E°_{ox}, the more favorable will be the kinetics of the reaction leading to the excited state (normal region) *and* the less favorable will be the kinetics of the reaction leading to the ground state (inverted region).[24,27]

Figure 7 suggests that (for a given coreactant) there is a critical value of E°_{ox} for each emission color, necessary for ECL to be observed (denoted $E_{critical}$). Figure 8 illustrates the location of the luminophores investigated in this study relative to these critical values, plotted as a line transecting a graph of oxidation potential versus emission color. We have termed the critical line the ECL "wall", as only complexes positioned to the right of the line will have reactions which are energy sufficient and thus exhibit ECL. The plot in Figure 8 well illustrates the issues discussed above: **15** gave the most intense ECL of the iridium complexes and is positioned relatively far from the "wall"; **14** gave very low ECL and is adjacent to the wall; **11**−**13** all fall on the energy-deficient side of the wall. For comparison, $Ru(bpy)_3^{2+}$, the benchmark ECL emitter, enjoys the position most remote from the "wall" on the energy-sufficient side, whereas $Ir(pmi)_3$ (tris(1-phenyl-3-methylimidazolin-2-ylidene-*C*,$C^{2'}$)iridium(III)), which is known from a previous study[24] to give no ECL despite a photoluminescence quantum yield approaching unity, has an oxidation potential of 0.22 V and an emission maximum of 405 nm and occupies the most unfavorable location on the graph from the point of view of ECL.

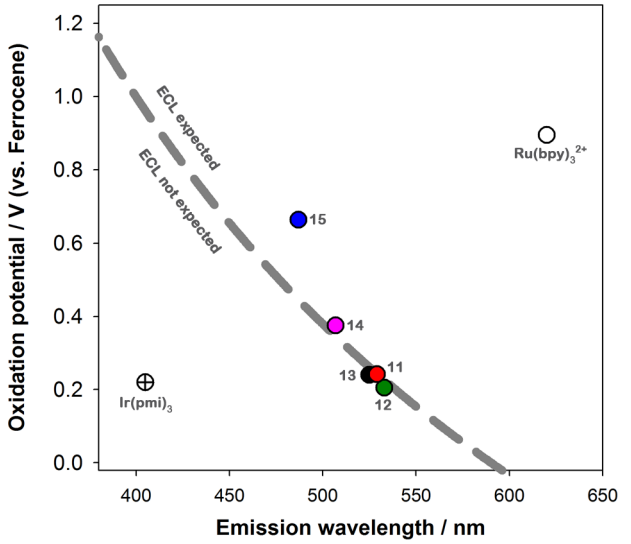

Figure 8. ECL wall of energy sufficiency for tripropylamine (TPA). The dashed line represents the critical oxidation potential required for ECL for a given emission color when TPA is the coreactant. Reactions of the TPA radical with compounds falling to the right of this line will be energy sufficient for excited state formation; reactions with compounds falling to the left of the line will not be energy sufficient.

It should be acknowledged that there are other determinants of ECL efficiency that are not taken into account by the graph, such as photoluminescence quantum yield and the kinetic stability of the oxidized form of the luminophore. However, this plot is proposed as a useful "ready reckoner" for predicting the likely ECL ability of compounds in the search for new electrochemiluminophores with differing emission colors.

CONCLUSION

A novel series of heteroleptic iridium(III) complexes with two cyclometalated 2-(phenyl)pyridine ligands in combination with a cyclometalated phenylimidazolylidene unit were synthesized. The phenyl group of the bidentate imidazolylidene unit was substituted at the 2- and 4-positions with electron-withdrawing and -donating substituents in an effort to modulate the electron density at the metal center. The precursor 2,4-disubsituted phenylimidazoles were prepared using a two-step procedure from the appropriate disubstituted aniline and glyoxal, followed by the addition of NH_4Cl and formaldehyde. Each of the iridium(III) complexes exhibited intense photoluminescence in acetonitrile solution at room temperature with quantum yields (ϕ_p) ranging from 42% to 68% and excited-state lifetimes on the order of 2 μs. These properties suggest possible applications in electroluminescent devices, as lifetimes are long enough for triplet exciton harvesting, yet short enough that triplet−triplet annihilation and quantum efficiency rolloff would be unlikely to diminish device performance.

Substitution at the phenyl ring of the auxiliary ligand can be effectively used to modulate the energy of the substantially metal based HOMO. For example, fluorine substituents at the 2- and 4-positions of this ligand bring about a 50 nm shift in emission wavelength. Similarly, the oxidation potentials of the complexes are sensitive to substitution on the auxiliary ligand but the reduction potentials are not. It can be surmised therefore that substitution at this position represents a good strategy for stabilizing HOMO levels while having a lesser or no effect on the LUMO, which is most remote from the substitution point in these complexes. DFT calculations confirm that the HOMO is delocalized over the iridium center and the phenyl rings of the phenylpyridine ligands and that the LUMO is largely localized on the pyridine moieties of the phenylpyridines.

All five complexes exhibited moderate to intense electrochemiluminescence (ECL) via the annihilation mechanism; however, only **15** produced significant coreactant ECL with tripropylamine (TPA). This can be understood as being a consequence of the relative oxidizing abilities of the complexes and by considering the energetics of the ECL reaction leading to the excited state. Generally it can be surmised that bluer emitters require more positive oxidation potentials in order to be coreactant ECL active. To this end, a plot of oxidation potential versus emission energy is proposed as a convenient guide to aid in the prediction of energy sufficiency in ECL reactions.

It is clear that when seeking to design electrochemiluminophores with bluer emission (larger HOMO−LUMO gap) the only fruitful strategies will involve stabilization of the HOMO levels (rather than destabilization of LUMO). Fortunately, because of the delocalized nature of the HOMO in iridium complexes of this type (as opposed to their ruthenium-based counterparts which have HOMOs almost exclusively localized

dx.doi.org/10.1021/om500076w | *Organometallics* 2014, 33, 4860−4872

on the metal), proven strategies exist for independently modifying the frontier orbital energies. For example, in the series of compounds studied here, the HOMO levels could be selectively stabilized by substitution of strongly electron withdrawing groups on the phenyl rings of the phenylpyridine ligands. In principle this should result in a more positive oxidation potential and greater ECL efficiency. We intend to explore this avenue in future work.

EXPERIMENTAL SECTION

General Considerations. All reagents were purchased from Sigma-Aldrich or Alfa Aesar and were of analytical grade or higher and were used without further purification unless otherwise stated. Dry acetonitrile was distilled from CaH_2. NMR spectra were recorded using a Bruker ARX-300 (300.14 MHz for ^1H, 75.48 MHz for ^{13}C) NMR spectrometer and were referenced to solvent resonances. Microanalyses were performed by the Microanalytical Laboratory at the ANU Research School of Chemistry, Canberra, Australia. All compounds were prepared in air unless otherwise specified.

Photophysical Measurements. UV−visible spectra were collected using a Cary Series UV−visible spectrophotometer (Agilent) with a 1 cm path length quartz cuvette, a spectral bandwidth of 1 nm, a signal averaging time of 0.1 s, a data interval of 0.25 nm, and a scan rate of 150 nm/min. Steady-state emission spectra were collected on a Nanolog (HORIBA Jobin Yvon IBH) spectrometer using a 1 cm quartz cuvette, a band pass of 2 nm, an increment of 1 nm, and an integration time of 0.2 s. One micromolar solutions in an airtight four-sided quartz cuvette were degassed with Ar in a N_2 glovebox for 10 min. A 450 W xenon-arc lamp was used to excite the complexes using a 1200 g/mm grating blazed at 330 nm excitation monochromators, a 1200 g/mm grating blazed at a 500 nm emission monchromator, and a thermoelectrically cooled TBX picosecond single-photon detector. Emission and excitation spectra were corrected for source intensity, gratings, and detector response. Lifetimes (5 μM solutions) were measured using the time correlated single photon counting (TCSPC) option on the spectrometer and correlated by a time-to-amplitude converter (TAC) in forward TAC mode. Nanoled 340 (344 nm) and Nanoled 460 (451 nm) lasers were pulsed at a 100 kHz repetition rate, and the emission bandwidth was set to 5 nm. Signals were collected using a FluoroHub counter and the data analyzed using DAS6 software (HORIBA Jobin Yvon IBH). Spectra for absolute quantum yields were measured at room temperature (22 ± 2 °C) with a Quanta-phi HORIBA Scientific 6 in. diameter integrating sphere connected to the Nanolog via optical fibers. The complexes were excited using a 450 W xenon lamp and detected with a liquid nitrogen cooled Symphony II (Model SII-1LS-256−06) CCD. Absolute quantum yields were calculated by the four-plot method using Fluoressence v3.5 software following the equation

$$\varphi_p = \frac{\text{photons out}}{\text{photons in}} = \frac{(E_c - E_a)/A}{L_a - L_c} \quad (10)$$

where E_c is the integrated luminescence of the sample, E_a is the integrated luminescence of the blank, A is the area factor due to CCD integration time, L_a is the integrated excitation from the blank, and L_c is the integrated excitation from the sample. Spectral measurements were averaged from at least six replicates. The 95% confidence intervals for the quantum yield measurements were no more than ±0.0035. For example, the quantum yield for $Ru(bpy)_3^{2+}$ was found to be 0.087 ± 0.002 at the 95% level of confidence (n = 6).

Electrochemistry. Electrochemical experiments were performed using a PGSTAT12 AUTOLAB electrochemical potentiostat (MEP Instruments, North Ryde, NSW, Australia) with Nova 1.8 software. A conventional three-electrode cell configuration was used, consisting of a silver-wire quasi reference electrode, a platinum-wire auxiliary electrode, and a 3 mm diameter glassy-carbon-disk working electrode shrouded in Teflon (CH Instruments, Austin, TX, USA). The working electrode was polished with 0.3 μm and then 0.05 μm alumina slurry on a felt pad, rinsed with Milli-Q water followed by acetone, and then sonicated in acetonitrile for 10 s followed by a final rinse in acetonitrile and dried with a stream of N_2. Potentials were referenced to the ferrocene/ferrocenium couple measured in situ (0.2 mM) in each case. Stock solutions of the complexes were prepared at a concentration of 0.2 mM in freshly distilled acetonitrile, and $[Bu_4N][PF_6]$ was added to give a concentration of 0.1 M of supporting electrolyte. Oxygen was removed from the solutions by bubbling vigorously with N_2 for 10 min followed by lightly blanketing the solution with N_2 during the experiments. Scan rates ranging from 0.01 to 0.5 V s^{-1} were used in cyclic voltammetry to evaluate the diffusion coefficients using the Randles−Sevçik equation (see Figure S3 in the Supporting Information).

Electrochemiluminescence (ECL). Relative ECL efficiencies (ϕ_{ECL}) were evaluated by comparison of the ECL spectra (annihilation) or PMT signal intensity (coreactant) with that of 0.2 mM $[Ru(bpy)_3]^{2+}$ in acetonitrile containing 0.1 M $[Bu_4N][PF_6]$.[28] Solutions were prepared with deoxygenated acetonitrile (freeze/pump/thaw three cycles) in a light-tight custom-made N_2 filled glovebox. Annihilation ECL was generated using chronoamperometry, where the cathodic and anodic potentials were stepped for 1.0 s sequentially for one cycle. An overpotential of 0.1 V was used to generate the 1+ and 1− forms of the Ir(III) complexes in the annihilation reactions. ECL spectra were obtained using a fiber optic (feed through from glovebox) to either an Ocean Optics CCD Model QE65 Pro (or QE6500 with the spectra smoothed) with a HR 4000 Breakout box trigger in conjunction with a μ-Autolab type II electrochemical station potentiostat (MEP Instruments, North Ryde, NSW, Australia).

Coreactant ECL was generated with a 3 mm diameter glassy-carbon electrode in a 0.2 mM solution of the complex containing 0.1 M $[Bu_4N][PF_6]$ supporting electrolyte and 10 mM tripropylamine (TPA) as the coreactant. The potential was pulsed 0.1 V beyond the complex's oxidation potential for 1.0 s. ECL intensity was detected using a photomultipler tube (Model H7826-01 No. 62340001 Hamamatsu Japan), biased by an input control voltage of 0.3 V using a power supply with a variable resistor. The output signal of the photomultiplier was acquired using the auxiliary channel of the potentiostat via a TA-GI-74 Ames Photonics Inc. amplifier (Model D7280).

Solution-phase ECL efficiencies (ϕ_{ECL}) were measured relative to $Ru(bpy)_3^{2+}$ taken as 100% and were evaluated using the equation

$$\varphi_{ECL} = IQ_f^s/Q_f I^s \quad (11)$$

where I and I^s are the integrated spectra (or PMT responses) for the sample and standard, respectively, and Q_f and Q_f^s are the total Faradaic charges passed during the forward step for the sample and standard, respectively.

Theoretical Calculations. Density functional theory (DFT) calculations were carried out within the Gaussian 09 suite of programs.[29] Ground state geometries were optimized in the absence of solvent with the mPW1PW91[30] functional in conjunction with the def2-SVP basis set and associated core potential.[31] The mPW1PW91 functional has previously been demonstrated to yield reliable results for such systems.[15f,32] M06-2X[33] optimized geometries were equivalent. Single-point energy calculations were carried out with the def2-TZVP basis set and core potential.[31] The polarizable continuum model (PCM)[34] self-consistent reaction field (SCRF) was used to model solvent effects at the gas-phase optimized geometries with a solvent of acetonitrile, consistent with the experimental system. Frontier MO energies were calculated using DFT MOs with mPW91PW91, PBE,[35] B3LYP,[36] BP86,[36a,37] M06-2X,[33] and wB97XD.[38] Diffuse basis functions for the def2-TZVP basis set were generated in an even-tempered manner; one additional function of each orbital angular momentum was generated using a ratio of 2.4 to the exponent of the most diffuse function in the original basis set. An SCF convergence criteria of 10^{-8} au was employed throughout, with the exception of the augmented basis set calculations that required a reduced threshold of 10^{-6} au (test calculations indicate the effect of reduced convergence criteria was in the order of 10^{-4} au in MO energies). TD-DFT calculations were carried out at the mPW1PW91/

dx.doi.org/10.1021/om500076w | Organometallics 2014, 33, 4860−4872

def2-TZVP level of theory with the SCRF PCM solvent field of acetonitrile; 30 singlet states were modeled. Molecular orbital analysis was carried out with the AOMix program.[39]

X-ray Crystallography. Single crystals of imidazolium salts **9** and **10** were grown by slow evaporation of methanol solutions of each compound. Single crystals of the Ir(III) complexes **12** and **15** suitable for X-ray diffraction studies were grown by slow evaporation of acetonitrile solutions of each compound. Crystallographic data for all structures determined are given in Table 1 and Table S1 (Supporting Information). For all samples, crystals were removed from the crystallization vial and immediately coated with Paratone oil on a glass slide. A suitable crystal was mounted in Paratone oil on a glass fiber and cooled rapidly to 173 K in a stream of cold N_2 using an Oxford low-temperature device. Diffraction data were measured using an Oxford Gemini diffractometer mounted with Mo Kα (λ = 0.71073 Å) and Cu Kα radiation (λ = 1.54184). Data were reduced and corrected for absorption using the CrysAlis Pro program.[5b] The SHELXL2013-2[40] program was used to solve the structures with direct methods, with refinement by full-matrix least-squares refinement techniques on F^2. The non-hydrogen atoms were refined anisotropically, and hydrogen atoms were placed geometrically and refined using the riding model. Coordinates and anisotropic thermal parameters of all non-hydrogen atoms were refined. All calculations were carried out using the program Olex2.[41] Images were generated by using ORTEP-3.[20] Further XRD details are provided in the Supporting Information. CCDC 982477−982480 contain supplementary crystallographic data for this paper. These data can be obtained free of charge from The Cambridge Crystallographic Data Centre via www.ccdc.cam.ac.uk/data_request/cif

Synthesis. These compounds were prepared using a modified literature procedure.[14d]

Compound ***1***. A mixture of aniline (9.13 mL, 0.1 mol), 40% glyoxal (4.2 mL, 0.1 mol), and CH_3OH (50 mL) was stirred for 18 h at room temperature to give a brown solution. NH_4Cl (10.7 g, 0.2 mol) was added followed by 37% formaldehyde (16 mL, 0.2 mol), and the mixture was diluted with CH_3OH (400 mL). The resulting mixture was refluxed for 1 h, and then H_3PO_4 (14 mL, 85%) was added dropwise over 30 min and the reflux was continued for a further 10 h. The solvent was then removed under reduced pressure, and ice-cold water (300 mL) was added followed by 40% aqueous KOH to raise the pH to 9. The mixture was extracted with ethyl acetate (5 × 150 mL), the organic extracts were washed with brine (100 mL) and dried with Mg_2SO_4, and the solvent was removed under reduced pressure. After purification on silica, with ethyl acetate/hexane (4/1 v/v) as the eluent, the product was obtained as a brown oil (yield: 9.01 g, 64%). ^{1}H NMR (DMSO): δ 7.12 (dd, 1H, $^3J_{HH}$ = 2.24 Hz, $^4J_{HH}$ = 1.2 Hz, H_{imi}), 7.35 (t, 1H, $^3J_{HH}$ = 7.4 Hz, H_{aryl}), 7.51 (t, 2H, $^3J_{HH}$ = 7.52 Hz, H_{aryl}), 7.64 (d, 2H, $^3J_{HH}$ = 8.60 Hz, H_{aryl}), 7.74 (dd, 1H, $^3J_{HH}$ = 2.72 Hz, $^4J_{HH}$ = 1.36 Hz, H_{imi}), 8.26 (t, 1H, $^4J_{HH}$ = 1.08 Hz, NC*H*N). ^{13}C NMR (DMSO): δ 118.44 (C_{imi}), 120.79 (2 × C_{aryl}), 127.31 (C_{aryl}), 130.30 (2 × C_{aryl}), 130.36 (C_{imi}), 135.97 (NCN), 137.40 (C_q). Anal. Found: C, 70.17; H, 5.95; N, 18.16. Calcd for $C_9H_8N_2{\cdot}0.5H_2O$: C, 70.57; H, 5.92; N, 18.29.

Compound ***2***. This compound was prepared as described for **1**, from 2,4-dimethylaniline (1.21 g, 0.01 mol), 40% glyoxal (4.2 mL, 0.1 mol), CH_3OH (7 mL), NH_4Cl (1.07 g, 0.02 mol), 37% formaldehyde (0.5 mL, 0.02 mol), and H_3PO_4 (0.15 mL, 85%). After purification the product was obtained as a dark brownish red oil (yield: 0.82 g, 48%). ^{1}H NMR ($CDCl_3$): δ 2.13 (s, 3H, CH_3), 2.37 (s, 3H, CH_3), 7.03 (t, 1H, $^3J_{HH}$ = 1.28 Hz, H_{imi}), 7.06−7.11 (m, 2H, H_{aryl}), 7.4 (t, 1H, $^3J_{HH}$ = 1.52 Hz, H_{aryl}), 7.20 (t, 1H,, $^3J_{HH}$ = 1.00 Hz, H_{imi}), 7.60 (s, 1H, NC*H*N). ^{13}C NMR ($CDCl_3$): δ 17.51 (CH_3), 21.04 (CH_3), 120.74 (C_{imi}), 126.36 (C_{aryl}), 127.48 (C_{aryl}), 128.83 (C_{imi}), 131.92 (C_{aryl}), 133.58 (C_q), 134.05 (C_q), 137.50 (NCN), 138.96 (C_q). Anal. Found: C, 72.46; H, 7.22; N, 15.33. Calcd for $C_{11}H_{12}N_2{\cdot}0.6H_2O$: C, 72.18; H, 7.27; N, 15.3.

Compound ***3***. This compound was prepared as described for **1**, from 2,4-dimethoxyaniline (1.53 g, 0.01 mol), 40% glyoxal (4.2 mL, 0.1 mol), CH_3OH (7 mL), NH_4Cl (1.07 g, 0.02 mol), 37% formaldehyde (0.5 mL, 0.02 mol), and H_3PO_4 (0.15 mL, 85%). After purification the product was obtained as a dark brown oil (yield: 1.08 g, 53%). ^{1}H NMR (d_6-DMSO): δ 3.80 (s, 3H, OCH_3), 3.81 (s, 3H, OCH_3), 6.62 (dd, 1H, $^3J_{HH}$ = 8.68 Hz, $^4J_{HH}$ = 2.64 Hz, H_{aryl}), 6.77 (d, 1H, $^3J_{HH}$ = 2.60 Hz, H_{aryl}), 7.00 (t, 1H, $^3J_{HH}$ = 1.81 Hz, H_{imi}), 7.28 (s, 1H, H_{aryl}), 7.30 (t, 1H, $^3J_{HH}$ = 3 Hz, H_{aryl}), 7.76 (t, 1H, $^3J_{HH}$ = 1.08 Hz, NC*H*N). ^{13}C NMR (d_6-DMSO): δ 55.58 (OCH_3), 55.96 (OCH_3), 99.72 (C_{aryl}), 105.06 (C_{aryl}), 119.36 (C_q), 120.86 (C_{imi}),126.52 (C_{aryl}), 128.05 (C_{imi}), δ 137.68 (NCN), 153.45 (C_q), 159.92 (C_q). Anal. Found: C, 61.89; H, 6.29; N, 13.20. Calcd for $C_{11}H_{12}N_2O_2{\cdot}0.5H_2O$: C, 61.96; H, 6.15; N, 13.14.

Compound ***4***. This compound was prepared as described for **1**, from 2,4-dichloroaniline (1.62 g, 0.01 mol), 40% glyoxal (4.2 mL, 0.1 mol), CH_3OH (7 mL), NH_4Cl (1.07 g, 0.02 mol), 37% formaldehyde (0.5 mL, 0.02 mol), and H_3PO_4 (0.15 mL, 85%). After purification the product was obtained as a dark brownish red oil (yield: 0.91 g, 43%). ^{1}H NMR (d_6-DMSO): δ 7.11 (dd, 1H, $^3J_{HH}$ = 1.2 Hz, $^4J_{HH}$ = 1 Hz, H_{imi}), 7.45 (dd, 1H, $^3J_{HH}$ = 1.28 Hz, $^4J_{HH}$ = 1.32 Hz, H_{imi}), 7.59−7.60 (m, 2H, H_{aryl}), 7.90−7.91 (m, 2H, H_{aryl}). ^{13}C NMR (d_6-DMSO): δ 121.40 (C_{imi}), 128.95 (C_{aryl}), 129.38 (C_{imi}), 130.01 (C_{aryl}), 130.07 (C_q), 130.44 (C_{aryl}), 134.17 (C_q), 134.39 (C_q), 138.24 (NCN). Anal. Found: C, 50.63; H, 2.79; N, 13.02. Calcd for $C_9H_6Cl_2N_2$: C, 50.74; H, 2.84; N, 13.15.

Compound ***5***. This compound was prepared as described for **1**, from 2,4-difluoroaniline (1.29 g, 0.01 mol), 40% glyoxal (4.2 mL, 0.1 mol), CH_3OH (7 mL), NH_4Cl (1.07 g, 0.02 mol), 37% formaldehyde (0.5 mL, 0.02 mol), and H_3PO_4 (0.15 mL, 85%). After purification on silica the product was obtained as a purple crystalline solid, and subsequent recrystallization from ether and hexane resulted in a colorless crystalline solid (yield: 0.89 g, 49%). ^{1}H NMR (d_6-DMSO): δ 7.12 (dd, 1H, $^3J_{HH}$ = 1.2 Hz, $^4J_{HH}$ = 1 Hz, H_{imi}), 7.25−7.30 (m, 1H, H_{aryl}), 7.53 (dd, 1H, $^3J_{HH}$ = 3 Hz, $^4J_{HH}$ = 1.4 Hz, H_{imi}), 7.56−7.61 (m, 1H, H_{aryl}), 7.71 (td, 1H, $^3J_{HH}$ = 5.9 Hz, $^3J_{HH}$ = 8.9 Hz H_{aryl}), 7.80 (s, 1H, NC*H*N). ^{13}C NMR (d_6-DMSO): δ 105.21 (C_q), 105.48 (C_{aryl}), 112.30 (C_{aryl}), 112.53 (C_q), 120.33 (C_{imi}), 121.88 (C_q), 127.37 (C_{aryl}), 129.17 (C_{imi}), 137.43 (NCN). Anal. Found: C, 60.00; H, 3.26; N, 15.46. Calcd for $C_9H_6F_2N_2$: C, 60.00; H, 3.36; N, 15.55.

Compound ***6***. A mixture of **1** (0.5 g, 3.47 mmol) and CH_3I (0.74 g, 5.2 mmol) in CH_3CN (20 mL) was refluxed for 18 h under N_2. The solvent was removed under reduced pressure, the crude product was recrystallized from acetone and ether, and the product was obtained as a pale cream-colored solid (yield: 0.79 g, 80%). ^{1}H NMR (d_6-DMSO): δ 3.95 (s, 3H, NCH_3), 7.60 (t, 1H, $^3J_{HH}$ = 8.0 Hz, H_{aryl}), 7.67 (t, 2H, $^3J_{HH}$ =13.5 Hz, H_{aryl}), 7.76 (d, 2H, $^3J_{HH}$ = 8.5 Hz, H_{aryl}), 7.95 (t, 1H, $^3J_{HH}$ = 1.8 Hz, H_{imi}), 8.29 (t, 1H, $^3J_{HH}$ = 1.9 Hz, H_{imi}), 9.75 (s, 1H, NC*H*N). ^{13}C NMR (d_6-DMSO): δ 36.14 (CH_3), 120.98 (C_{imi}), 121.81 (2 × C_{aryl}), 124.42 (C_{imi}), 129.75 (C_{aryl}), 130.20 (2 × C_{aryl}), 134.73 (C_q), 135.96 (NCN). Anal. Found: C, 40.89; H, 3.80; N, 9.33. Calcd for $C_{10}H_{11}IN_2{\cdot}0.5H_2O$: C, 40.70; H, 4.10; N, 9.49.

Compound ***7***. This compound was prepared as described for **6**, from **2** (0.5 g, 2.9 mmol) and CH_3I (0.62 g, 4.4 mmol) in CH_3CN (20 mL). The crude product was recrystallized from acetone and ethyl acetate, and the product was obtained as a white crystalline solid (yield: 0.78 g, 86%). ^{1}H NMR ($CDCl_3$): δ 2.26 (s, 3H, CCH_3), 2.39 (s, 3H, CCH_3), 4.31 (s, 3H, NCH_3), 7.16 (d, 1H, $^3J_{HH}$ = 8.04 Hz, H_{aryl}), 7.19 (s, 1H, H_{aryl}), 7.31 (t, 1H, $^3J_{HH}$ = 1.81 Hz, H_{imi}), 7.34 (d, 1H, $^3J_{HH}$ = 8 Hz, H_{aryl}), 7.71 (t, 1H, $^3J_{HH}$ = 1.72 Hz, H_{imi}), 10.09 (s, 1H, NC*H*N). ^{13}C NMR ($CDCl_3$): δ 17.91 (CCH_3), 21.14 (CCH_3), 37.67 (NCH_3), 123.21 (C_{imi}), 123.98 (C_{imi}), 126.10 (C_{aryl}), 128.37 (C_{aryl}), 131.15 (C_q), 132.61 (C_{aryl}). 132.83 (C_q), 137.76 (NCN), 141.59 (C_q). Anal. Found: C, 45.95; H, 4.90; N, 9.09. Calcd for $C_{10}H_{16}IN_2$: C, 45.73; H, 5.12; N, 8.89.

Compound ***8***. This compound was prepared as described for **6**, from **3** (0.5 g, 2.45 mmol) and CH_3I (0.52 g, 3.68 mmol) in CH_3CN (20 mL). The crude product was recrystallized from acetone and ethyl acetate, and the product was obtained as a brown crystalline solid (yield: 0.65 g, 77%). ^{1}H NMR ($CDCl_3$): δ 3.86 (s, 3H, OCH_3), 3.89 (s, 3H, OCH_3), 4.27 (s, 3H, NCH_3), 6.60−6.62 (m, 2H, H_{aryl}), 7.44 (t, 1H, $^3J_{HH}$ = 1.8 Hz, H_{imi}), 7.56 (d, 1H, $^3J_{HH}$ = 7.14 Hz, H_{aryl}), 7.60 (t, 1H, $^3J_{HH}$ = 1.76 Hz, H_{imi}), 9.97 (s, 1H, NC*H*N). ^{13}C NMR ($CDCl_3$): δ 37.61 (CH_3), 56.00 (OCH_3), 56.48 (OCH_3), 100.03 (C_{aryl}), 105.45

dx.doi.org/10.1021/om500076w | *Organometallics* 2014, 33, 4860−4872

(C_{aryl}), 116.52 (C_q), 123.17 (C_{imi}), 123.46 (C_{imi}), 126.90 (C_{aryl}), 137.55 (NCN), 153.31 (C_q), 162.44 (C_q). Anal. Found: C, 41.72; H, 4.78; N, 8.14. Calcd for $C_{12}H_{16}IN_2O_2$: C, 41.52; H, 4.65; N, 8.07.

Compound 9. This compound was prepared as described for **6**, from **4** (0.45 g, 2.1 mmol) and CH_3I (0.45 g, 3.18 mmol) in CH_3CN (20 mL). The crude product was recrystallized from acetone and ether, and the product was obtained as a white crystalline solid (yield: 0.59 g, 79%). ^{1}H NMR ($CDCl_3$): δ 4.27 (s, 3H, NCH_3), 7.45 (t, 1H, $^3J_{HH}$ = 1.84 Hz, H_{imi}), 7.48 (d, 1H, $^3J_{HH}$ = 2.2 Hz, H_{aryl}), 7.60 (s, 1H, H_{aryl}), 7.67 (t, 1H, $^3J_{HH}$ = 1.8 Hz, H_{imi}), 7.96 (d, 1H, $^3J_{HH}$ = 6 Hz, H_{aryl}), 10.19 (s, 1H, NC*H*N). ^{13}C NMR ($CDCl_3$): δ 37.92 (CH_3), 123.38 (C_{imi}), 124.00 (C_{imi}), 129.35 (C_{aryl}), 129.61 (C_{aryl}), 130.15 (C_q), 130.51 (C_q), 130.97 (C_{aryl}), 138.19 (C_q), 138.38 (NCN). Anal. Found: C, 33.88; H, 2.60; N, 8.09. Calcd for $C_{10}H_{10}Cl_2IN_2$: C, 33.74; H, 2.83; N, 7.87.

Compound 10. This compound was prepared as described for **6**, from **5** (0.5 g, 2.77 mmol) and CH_3I (0.59 g, 4.17 mmol) in CH_3CN (20 mL). The crude product was recrystallized from acetone and ether, and the product was obtained as a purplish white crystalline solid (yield: 0.73 g, 82%). ^{1}H NMR ($CDCl_3$): δ 4.27 (s, 3H, NCH_3), 7.05−7.14 (m, 2H, H_{aryl}), 7.56 (dd, 1H, $^3J_{HH}$ = 3.76 Hz, $^4J_{HH}$ = 1.88 Hz, H_{imi}), 7.70 (t, 1H, $^3J_{HH}$ = 1.76 Hz, H_{imi}), 8.10 (td, 1H, $^3J_{HH}$ = 8.46 Hz, $^4J_{HH}$ = 5.36 Hz, H_{aryl}), 10.36 (s, 1H, NC*H*N). ^{13}C NMR ($CDCl_3$): δ 37.83 (CH_3), 105.75 (C_q), 106.01 (C_{aryl}), 106.25 (C_q), 113.48 (C_{aryl}), 113.71 (C_q), 122.80 (C_{imi}), 124.25 (C_{imi}), 128.16 (C_{aryl}), 137.73 (NCN). Anal. Found: C, 37.40; H, 2.90; N, 8.79. Calcd for $C_{10}H_{10}F_2IN_2$: C, 37.17; H, 3.12; N, 8.67.

Complex 11. A mixture of **6** (0.15 g, 0.52 mmol), Ag_2O (0.182 g, 0.79 mmol), and $[Ir(ppy)_2Cl]_2$ (0.28 g, 0.26 mmol) in 1,2-dichloroethane (15 mL) was heated in the dark at 100 °C under N_2. The hot reaction mixture was filtered through Celite, and the solvent was removed under reduced pressure. The crude product was recrystallized from CH_3CN and CH_2Cl_2, and the product was obtained as a yellow solid (yield: 0.30 g, 87%). ^{1}H NMR (d_6-DMSO): δ 3.06 (s, 3H, CH_3), 6.24 (d, 1H, J = 6.2 Hz), 6.55−6.64 (m, 3H), 6.73−6.78 (m, 2H), 6.80−6.95 (m, 3H), 6.93 (dd, 2H, J = 6.1 Hz, J = 1.24 Hz), 7.16 (d, 1H, J = 1.9 Hz), 7.38 (d, 1H, J = 7.7 Hz), 7.64−7.74 (m, 3H), 7.80 (d, 1H, J = 7.5 Hz), 7.88 (d, 1H, J = 5.5 Hz), 7.97−8.00 (m, 3H), 8.05 (d, 1H, J = 8.1 Hz). ^{13}C NMR (d_6-DMSO) δ 36.59, 111.27, 116.34, 119.27, 119.35, 119.66, 119.88, 121.85, 122.49, 122.79, 123.13, 124.45, 124.73, 125.30, 129.01, 129.31, 130.53, 132.88, 135.14, 135.81, 138.54, 143.88, 144.64, 148.91, 152.59, 152.87, 156.15, 168.46, 169.77, 172.23, 172.66, 176.21. Anal. Found: C, 58.33; H, 3.62; N, 8.32. Calcd for $C_{32}H_{25}IrN_4$: C, 58.43; H, 3.83; N, 8.52.

Complex 12. This complex was prepared as described for **11**, from **7** (0.15 g, 0.48 mmol), Ag_2O (0.166 g, 0.72 mmol), and $[Ir(ppy)_2Cl]_2$ (0.256 g, 0.24 mmol) in 1,2-dichloroethane (15 mL). The crude product was recrystallized from CH_3CN, and the product was obtained as a brownish orange solid (yield: 0.24 g, 73%). ^{1}H NMR ($CDCl_3$, 500 MHz): δ 2.07 (s, 3H, CH_3), 2.63 (s, 3H, CH_3), 3.13 (s, 3H, CH_3), 6.37 (d, 1H, J = 7.0 Hz), 6.52 (s, 1H), 6.63−6.73 (m, 4H), 6.79−6.89 (m, 4H), 7.46 (t, 1H, J = 7.5 Hz), 7.51 (t, 1H, J = 7.5 Hz), 7.65 (dd, 2H, J = 8 Hz, J = 4 Hz), 7.76−7.82 (m, 4H), 8.09 (d, 1H, J = 6 Hz). ^{13}C NMR ($CDCl_3$ - 500 MHz): δ 20.83, 21.98, 37.18, 118.19, 118.73, 118.89, 119.37, 119.43, 120.15, 120.18, 121.34, 121.61, 123.86, 123.98, 126.87, 129.00, 129.40, 130.40, 132.97, 133.65, 134.13, 134.23, 138.39, 143.18, 144.14, 145.37, 152.30, 153.19, 158.02, 169.15, 170.13, 173.36, 173.72, 178.36. Anal. Found: C, 58.72; H, 4.64; N, 8.07. Calcd for $C_{34}H_{29}IrN_4{\cdot}0.5H_2O$: C, 58.77; H, 4.35; N, 8.06.

Complex 13. This complex was prepared as described for **11**, from **8** (0.1 g, 0.29 mmol), Ag_2O (0.1 g, 0.43 mmol), and $[Ir(ppy)_2Cl]_2$ (0.155 g, 0.15 mmol) in 1,2-dichloroethane (15 mL). The crude product was recrystallized from hot CH_3CN, and the product was obtained as a greenish yellow solid (yield: 0.088 g, 42%). ^{1}H NMR (d_6-DMSO, 400 MHz): δ 3.04 (s, 3H, CH_3), 3.42 (s, 3H, CH_3), 3.85 (s, 3H, CH_3), 5.76 (d, 1H, J = 2.5 Hz), 6.15 (d, 1H, J = 2.5 Hz), 6.21 (dd, 1H, J = 6.4 Hz, J = 1 Hz), 6.54 (dd, 1H, J = 6.3 Hz, J = 0.9 Hz), 6.73−6.77 (m, 2H), 6.78−6.83 (m, 2H), 6.93−6.97 (m, 2H), 7.05 (d, 1H, J = 2.0 Hz), 7.65−7.32 (m, 3H), 7.81 (d, 2H, J = 6.5 Hz), 8.00 (d, 2H, J = 7.3 Hz), 8.05 (d, 1H, J = 8.4 Hz), 8.11 (d, 1H, J = 2.0 Hz). ^{13}C NMR (d_6-DMSO): 36.79, 54.72, 55.65, 92.32, 116.21, 119.26, 119.39, 119.71, 119.84 (2× *C*), 121.21, 122.57, 123.13, 124.37, 124.73, 128.98, 129.26, 129.99, 130.53, 132.87, 135.20, 135.77, 143.99, 144.53, 147.48, 152.50, 152.78, 157.80, 160.46, 168.53, 169.65, 172.80, 173.03, 174.82. Anal. Found: C, 56.08; H, 4.38; N, 7.08. Calcd for $C_{34}H_{29}IrN_4O_2{\cdot}CH_3OH$: C, 56.06; H, 4.44; N, 7.47.

Complex 14. This complex was prepared as described for **11**, from **9** (0.15 g, 0.42 mmol), Ag_2O (0.149 g, 0.65 mmol), and $[Ir(ppy)_2Cl]_2$ (0.23 g. 0.22 mmol) in 1,2-dichloroethane (15 mL). The crude product was recrystallized from in CH_2Cl_2 and CH_3CN, and the product was obtained as a yellow solid (yield: 0.267 g, 86%). ^{1}H NMR (d_6-DMSO): δ 3.08 (s, 3H, CH_3), 6.16 (d, 1H, J = 6.24 Hz), 6.43−6.46 (m, 2H), 6.74−6.88 (m, 4H), 6.98−7.44 (m, 3H), 7.23 (d, 1H, J = 2.20 Hz), 7.72−7.79 (m, 3H), 7.81−7.86 (m, 3H), 8.08 (dd, 2H, J = 7.84 Hz, J = 7.32 Hz), 8.50 (d, 1H, J = 2.16 Hz). ^{13}C NMR (d_6-DMSO): δ 37.09, 117.63, 119.65, 119.80, 120.33, 120.44, 122.65, 123.07, 123.40, 123.62, 124.79, 124.90, 129.26, 129.82, 129.95, 130.29, 132.48, 136.00, 136.12, 136.36, 143.30, 143.84, 144.32, 152.33, 152.91, 165.01, 168.25, 169.37, 170.61, 171.74, 178.47. Anal. Found: C, 51.09; H, 3.15; N, 7.34. Calcd for $C_{32}H_{23}Cl_2IrN_4{\cdot}1.5H_2O$: C, 50.99; H, 3.48; N, 7.43.

Complex 15. This complex was prepared as described for **11**, from **10** (0.1 g, 0.31 mmol), Ag_2O (0.11 g, 467 mmol), and $[Ir(ppy)_2Cl]_2$ (0.166 g, 0.155 mmol) in 1,2-dichloroethane (15 mL). The crude product was recrystallized in CH_3CN, and the desired product was obtained as a greenish yellow solid (yield: 0.08 g, 38%). ^{1}H NMR (d_6-DMSO): δ 3.08 (s, 3H, CH_3), 6.08 (dd, 1H, J = 5.24 Hz, J = 2.48), 6.21 (d, 1H, J = 6.88 Hz), 6.50 (d, 1H, J = 7.00 Hz), 6.66 (t, 1H, J = 10.42 Hz), 6.75−6.88 (m, 4H), 6.99 (t, 2H, J = 5.80 Hz), 7.21 (d, 1H, J = 1.92 Hz), 7.70−7.78 (m, 3H), 7.81−7.87 (m, 4H), 8.07 (dd, 2H, J = 9.52 Hz, J = 8.28 Hz). ^{13}C NMR (d_6-DMSO): δ 36.81, 118.60, 118.78, 118.93, 119.09, 119.54, 119.65, 120.26, 120.28, 122.97, 123.25, 123.30, 123.54, 124.65, 124.85, 129.19, 12.64, 130.39, 131.14, 132.59, 135.86, 136.27, 144.02, 144.45, 152.37, 152.97, 164.64, 168.31, 169.46, 170.31, 171.08, 176.32. Anal. Found: C, 55.43; H, 3.45; N, 8.27. Calcd for $C_{32}H_{23}F_2IrN_4$: C, 55.40; H, 3.34; N, 8.08.

■ ASSOCIATED CONTENT

Supporting Information

Text, a table, figures, and CIF and .xyz files giving further information on X-ray crystallography, X-ray crystallographic data for **9**, **10**, **12**, and **15**, photoluminescence and electrochemistry data, optimized geometry plots of molecular orbitals and plots of fragment contributions to frontier MOs and all computed molecule Cartesian coordinates in a format for convenient visualization. This material is available free of charge via the Internet at http://pubs.acs.org.

■ AUTHOR INFORMATION

Corresponding Authors

*E-mail for P.J.B.: p.barnard@latrobe.edu.au.
*E-mail for C.F.H.: c.hogan@latrobe.edu.au.

Author Contributions

†These authors contributed equally.

Notes

The authors declare no competing financial interest.

■ ACKNOWLEDGMENTS

This work was funded by the Australian Research Council (LE120100213 and DP1094179). We thank the Victorian Partnership for Advanced Computing (VPAC), the National Computational Infrastructure National Facility (NCI-NF), and La Trobe University for computing resources.

REFERENCES

(1) Bourissou, D.; Guerret, O.; Gabbai, F.; Bertrand, G. *Chem. Rev.* **2000**, *100*, 39−92.
(2) Herrmann, W. A.; Goossen, L. J.; Spiegler, M. *Organometallics* **1998**, *17*, 2162−2168.
(3) Hitchcock, P. B.; Lappert, M. F.; Terreros, P. *J. Organomet. Chem.* **1982**, *239*, C26−C30.
(4) Mercs, L.; Albrecht, M. *Chem. Soc. Rev.* **2010**, *39*, 1903−1912.
(5) (a) Son, S. U.; Park, K. H.; Lee, Y.-S.; Kim, B. Y.; Choi, C. H.; Lah, M. S.; Jang, Y. H.; Jang, D.-J.; Chung, Y. K. *Inorg. Chem.* **2004**, *43*, 6896−6898. (b) Chen, H.-S.; Chang, W.-C.; Su, C.; Li, T.-Y.; Hsu, N.-M.; Tingare, Y. S.; Li, C.-Y.; Shie, J.-H.; Li, W.-R. *Dalton Trans.* **2011**, *40*, 6765−6770. (c) Dinda, J.; Liatard, S.; Chauvin, J.; Jouvenot, D.; Loiseau, F. *Dalton Trans.* **2011**, *40*, 3683−3688. (d) Lee, C.-S.; Zhuang, R. R.; Wang, J.-C.; Hwang, W.-S.; Lin, I. J. B. *Organometallics* **2012**, *31*, 4980−4987. (e) Chang, W.-C.; Chen, H.-S.; Li, T.-Y.; Hsu, N.-M.; Tingare, Y. S.; Li, C.-Y.; Liu, Y.-C.; Su, C.; Li, W.-R. *Angew. Chem., Int. Ed.* **2010**, *49*, 8161−8164. (f) Barbante, G. J.; Francis, P. S.; Hogan, C. F.; Kheradmand, P. R.; Wilson, D. J. D.; Barnard, P. J. *Inorg. Chem.* **2013**, *52*, 7448−7459.
(6) (a) Unger, Y.; Zeller, A.; Ahrens, S.; Strassner, T. *Chem. Commun.* **2008**, 3263−3265. (b) Unger, Y.; Zeller, A.; Taige, M. A.; Strassner, T. *Dalton Trans.* **2009**, 4786−4794. (c) Lee, C.-S.; Sabiah, S.; Wang, J.-C.; Hwang, W.-S.; Lin, I. J. B. *Organometallics* **2009**, *29*, 286−289. (d) Unger, Y.; Meyer, D.; Strassner, T. *Dalton Trans.* **2010**, *39*, 4295−4301. (e) Unger, Y.; Meyer, D.; Molt, O.; Schildknecht, C.; Münster, I.; Wagenblast, G.; Strassner, T. *Angew. Chem., Int. Ed.* **2010**, *49*, 10214−10216. (f) Sun, R. W.-Y.; Chow, A. L.-F.; Li, X.-H.; Yan, J. J.; Chui, S. S.-Y.; Che, C.-M. *Chem. Sci.* **2011**, *2*, 728−736.
(7) (a) Casson, L. A.; Muzzioli, S.; Raiteri, P.; Skelton, B. W.; Stagni, S.; Massi, M.; Brown, D. H. *Dalton Trans.* **2011**, *40*, 11960−11967. (b) Li, X.-W.; Li, H.-Y.; Wang, G.-F.; Chen, F.; Li, Y.-Z.; Chen, X.-T.; Zheng, Y.-X.; Xue, Z.-L. *Organometallics* **2012**, *31*, 3829−3835.
(8) (a) Barnard, P. J.; Baker, M. V.; Berners-Price, S. J.; Skelton, B. W.; White, A. H. *Dalton Trans.* **2004**, 1038−1047. (b) Barnard, P. J.; Wedlock, L. E.; Baker, M. V.; Berners-Price, S. J.; Joyce, D. A.; Skelton, B. W.; Steer, J. H. *Angew. Chem., Int. Ed.* **2006**, *45*, 5966−5970. (c) Catalano, V. J.; Etogo, A. O. *J. Organomet. Chem.* **2005**, *690*, 6041−6050.
(9) (a) Holmes, R. J.; Forrest, S. R.; Sajoto, T.; Tamayo, A.; Djurovich, P. I.; Thompson, M. E.; Brooks, J.; Tung, Y.-J.; D'Andrade, B. W.; Weaver, M. S.; Kwong, R. C.; Brown, J. J. *Appl. Phys. Lett.* **2005**, *87*, 243507. (b) Sajoto, T.; Djurovich, P. I.; Tamayo, A.; Yousufuddin, M.; Bau, R.; Thompson, M. E.; Holmes, R. J.; Forrest, S. R. *Inorg. Chem.* **2005**, *44*, 7992−8003.
(10) Chien, C.-H.; Fujita, S.; Yamoto, S.; Hara, T.; Yamagata, T.; Watanabe, M.; Mashima, K. *Dalton Trans.* **2008**, 916−923.
(11) Chang, C.-F.; Cheng, Y.-M.; Chi, Y.; Chiu, Y.-C.; Lin, C.-C.; Lee, G.-H.; Chou, P.-T.; Chen, C.-C.; Chang, C.-H.; Wu, C.-C. *Angew. Chem., Int. Ed.* **2008**, *47*, 4542−4545.
(12) Lu, K.-Y.; Chou, H.-H.; Hsieh, C.-H.; Yang, Y.-H. O.; Tsai, H.-R.; Tsai, H.-Y.; Hsu, L.-C.; Chen, C.-Y.; Chen, I. C.; Cheng, C.-H. *Adv. Mater.* **2011**, *23*, 4933−4937.
(13) (a) Zhang, F.; Duan, L.; Qiao, J.; Dong, G.; Wang, L.; Qiu, Y. *Org. Electron.* **2012**, *13*, 1277−1288. (b) Kessler, F.; Costa, R. D.; Di Censo, D.; Scopelliti, R.; Orti, E.; Bolink, H. J.; Meier, S.; Sarfert, W.; Gratzel, M.; Nazeeruddin, M. K.; Baranoff, E. *Dalton Trans.* **2012**, *41*, 180−191. (c) Monti, F.; Kessler, F.; Delgado, M.; Frey, J.; Bazzanini, F.; Accorsi, G.; Armaroli, N.; Bolink, H. J.; Ortí, E.; Scopelliti, R.; Nazeeruddin, M. K.; Baranoff, E. *Inorg. Chem.* **2013**, *52*, 10292−10305.
(14) (a) Barbante, G. J.; Hogan, C. F.; Mechler, A.; Hughes, A. B. *J. Mater. Chem.* **2010**, *20*, 891−899. (b) Forster, R. J.; Bertoncello, P.; Keyes, T. E. *Annu. Rev. Anal. Chem.* **2009**, *2*, 359−385. (c) Miao, W. *Chem. Rev.* **2008**, *108*, 2506−2553. (d) Liu, J.; Chen, J.; Zhao, J.; Zhao, Y.; Li, L.; Zhang, H. *Synthesis* **2003**, *2003*, 2661−2666. (e) Tennyson, A. G.; Rosen, E. L.; Collins, M. S.; Lynch, V. M.; Bielawski, C. W. *Inorg. Chem.* **2009**, *48*, 6924−6933. (f) Piper, D.; Barbante, G.; Brack, N.; Pigram, P.; Hogan, C. *Langmuir* **2011**, *27*, 474−480. (g) Joshi, T.; Barbante, G. J.; Francis, P. S.; Hogan, C. F.; Bond, A. M.; Gasser, G.; Spiccia, L. *Inorg. Chem.* **2012**, *51*, 3302−3315. (h) Joshi, T.; Barbante, G. J.; Francis, P. S.; Hogan, C. F.; Bond, A. M.; Spiccia, L. *Inorg. Chem.* **2011**, *50*, 12172−12183.
(15) (a) Bard, A. J. *Electrogenerated Chemiluminescence*; Marcel Dekker: New York, 2004; p 540. (b) Richter, M. M. *Chem. Rev.* **2004**, *104*, 3003−3036. (c) Gorman, B. A.; Francis, P. S.; Barnett, N. W. *Analyst* **2006**, *131*, 616−639. (d) Forster, R. J.; Bertoncello, P.; Keyes, T. E. *Annu. Rev. Anal. Chem.* **2009**, *2*, 359−385. (e) Hu, L.; Xu, G. *Chem. Soc. Rev.* **2010**, *39*, 3275−3304. (f) Barbante, G. J.; Hogan, C. F.; Wilson, D. J. D.; Lewcenko, N. A.; Pfeffer, F. M.; Barnett, N. W.; Francis, P. S. *Analyst* **2011**, *136*, 1329−1338. (g) Forster, R. J.; Keyes, T. E. *Neuromethods* **2013**, *80*, 347−367.
(16) Gross, E. M.; Armstrong, N. R.; Wightman, R. M. *J. Electrochem. Soc.* **2002**, *149*, E137−E142.
(17) Bruce, D.; Richter, M. M. *Anal. Chem.* **2002**, *74*, 1340−1342.
(18) (a) Kapturkiewicz, A.; Angulo, G. *Dalton Trans.* **2003**, 3907−3913. (b) Kapturkiewicz, A.; Chen, T.-M.; Laskar, I. R.; Nowacki, J. *Electrochem. Commun.* **2004**, *6*, 827−831. (c) Kapturkiewicz, A.; Nowacki, J.; Borowicz, P. *Electrochim. Acta* **2005**, *50*, 3395−3400. (d) Kapturkiewicz, A.; Nowacki, J.; Borowicz, P. *Z. Phys. Chem.* **2006**, *220*, 525.
(19) Garces, F. O.; King, K. A.; Watts, R. J. *Inorg. Chem.* **1988**, *27*, 3464−3471.
(20) Farrugia, L. *J. Appl. Crystallogr.* **1997**, *30*, 565.
(21) (a) Tamayo, A. B.; Alleyne, B. D.; Djurovich, P. I.; Lamansky, S.; Tsyba, I.; Ho, N. N.; Bau, R.; Thompson, M. E. *J. Am. Chem. Soc.* **2003**, *125*, 7377−7387. (b) Kiran, R. V.; Hogan, C. F.; James, B. D.; Wilson, D. J. D. *Eur. J. Inorg. Chem.* **2011**, 4816−4825.
(22) Sajoto, T.; Djurovich, P. I.; Tamayo, A. B.; Oxgaard, J.; Goddard, W. A.; Thompson, M. E. *J. Am. Chem. Soc.* **2009**, *131*, 9813−9822.
(23) Doeven, E. H.; Zammit, E. M.; Barbante, G. J.; Francis, P. S.; Barnett, N. W.; Hogan, C. F. *Chem. Sci.* **2013**, *4*, 977−982.
(24) Barbante, G. J.; Doeven, E. H.; Kerr, E.; Connell, T. U.; Donnelly, P. S.; White, J. M.; Lópes, T.; Laird, S.; Wilson, D. J.; Barnard, P. J.; Hogan, C. F.; Francis, P. S. *Chem. Eur. J.* **2014**, *20*, 3322−3332.
(25) Miao, W.; Choi, J.-P.; Bard, A. J. *J. Am. Chem. Soc.* **2002**, *124*, 14478−14485.
(26) Doeven, E. H.; Barbante, G. J.; Kerr, E.; Hogan, C. F.; Endler, J. A.; Francis, P. S. *Anal. Chem.* **2014**, *86*, 2727−2732.
(27) Marcus, R. A. *J. Chem. Phys.* **1956**, *24*, 966−978.
(28) Wallace, W. L.; Bard, A. J. *J. Phys. Chem.* **1979**, *83*, 1350−7.
(29) Frisch, M. J.; Trucks, G. W.; Schlegel, H. B.; Scuseria, G. E.; Robb, M. A.; Cheeseman, J. R.; Scalmani, G.; Barone, V.; Mennucci, B.; Petersson, G. A.; Nakatsuji, H.; Caricato, M.; Li, X.; Hratchian, H. P.; Izmaylov, A. F.; Bloino, J.; Zheng, G.; Sonnenberg, J. L.; Hada, M.; Ehara, M.; Toyota, K.; Fukuda, R.; Hasegawa, J.; Ishida, M.; Nakajima, T.; Honda, Y.; Kitao, O.; Nakai, H.; Vreven, T.; Montgomery, J. A., Jr.; Peralta, J. E.; Ogliaro, F.; Bearpark, M.; Heyd, J. J.; Brothers, E.; Kudin, K. N.; Staroverov, V. N.; Kobayashi, R.; Normand, J.; Raghavachari, K.; Rendell, A.; Burant, J. C.; Iyengar, S. S.; Tomasi, J.; Cossi, M.; Rega, N.; Millam, J. M.; Klene, M.; Knox, J. E.; Cross, J. B.; Bakken, V.; Adamo, C.; Jaramillo, J.; Gomperts, R.; Stratmann, R. E.; Yazyev, O.; Austin, A. J.; Cammi, R.; Pomelli, C.; Ochterski, J. W.; Martin, R. L.; Morokuma, K.; Zakrzewski, V. G.; Voth, G. A.; Salvador, P.; Dannenberg, J. J.; Dapprich, S.; Daniels, A. D.; Farkas, Ö.; Foresman, J. B.; Ortiz, J. V.; Cioslowski, J.; Fox, D. J. *Gaussian 09, Revision A.1*; Gaussian, Inc., Wallingford, CT, 2009.
(30) (a) Adamo, C.; Barone, V. *J. Chem. Phys.* **1998**, *108*, 664−675. (b) Perdew, J. P., Unified Theory of Exchange and Correlation Beyond the Local Density Approximation. In *Electronic Structure of Solids '91*; Ziesche, P., Eschrig, H., Eds.; Akademie Verlag: Berlin, 1991; pp 11−20.
(31) Weigend, F.; Ahlrichs, R. *Phys. Chem. Chem. Phys.* **2005**, *7*, 3297−3305.
(32) Lin, J.; Wu, K.; Zhang, M. *J. Comput. Chem.* **2009**, *30*, 2056−2063.
(33) Zhao, Y.; Truhlar, D. G. *Theor. Chem. Acc.* **2008**, *120*, 215−241.

(34) Tomasi, J.; Mennucci, B.; Cammi, R. *Chem. Rev.* **2005**, *105*, 2999−3093.
(35) (a) Perdew, J. P.; Burke, K.; Ernzerhof, M. *Phys. Rev. Lett.* **1996**, *77*, 3865−3868. (b) Perdew, J. P.; Burke, K.; Ernzerhof, M. *Phys. Rev. Lett.* **1997**, *78*, 1396.
(36) (a) Becke, A. D. *Phys. Rev. A: Gen. Phys.* **1988**, *38*, 3098−3100. (b) Becke, A. D. *J. Chem. Phys.* **1993**, *98*, 5648−5652. (c) Lee, C.; Yang, W.; Parr, R. G. *Phys. Rev. B: Condens. Matter* **1988**, *37*, 785−789.
(37) Perdew, J. P. *Phys. Rev. B* **1986**, *33*, 8822−8824.
(38) Chai, J.-D.; Head-Gordon, M. *Phys. Chem. Chem. Phys.* **2008**, *10*, 6615−6620.
(39) Gorelsky, S. I. *AOMix: Program for Molecular Orbital Analysis, Version 6.46*; University of Ottawa, Ottawa, Canada, 2010; http://www.sg-chem.net/, .
(40) Sheldrick, G. *Acta Crystallogr., Sect. A* **2008**, *64*, 112−122.
(41) Dolomanov, O. V.; Bourhis, L. J.; Gildea, R. J.; Howard, J. A. K.; Puschmann, H. *J. Appl. Crystallogr.* **2009**, *42*, 339−341.